

Tests and model calibration of high-strength steel tubular beam-to-column and column-base composite joints for moment-resisting structures

Raffaele Pucinotti^{1,*†}, Nicola Tondini², Gabriele Zanon² and Oreste S. Bursi²

¹Department of Architectural and Urban Patrimony, Mediterranean University of Reggio Calabria, Reggio Calabria, Italy

²Department of Civil, Environmental and Mechanical Engineering, Trento University, Trento, Italy

SUMMARY

Performance-based engineering (PBE) methodologies allow for the design of more reliable earthquake-resistant structures. Nonetheless, to implement PBE techniques, accurate finite element models of critical components are needed. With these objectives in mind, initially, we describe an experimental study on the seismic behaviour of both beam-to-column (BTC) and column-base (CB) joints made of high-strength steel S590 circular columns filled with concrete. These joints belonged to moment-resisting frames (MRFs) that constituted the lateral-force-resisting system of an office building. BTC joints were conceived as rigid and of partial strength, whereas CB joints were designed as rigid and of full strength. Tests on a BTC joint composed of an S275 steel composite beam and high-strength steel concrete-filled tubes were carried out. Moreover, two seismic CB joints were tested with stiffeners welded to the base plate and anchor bolts embedded in the concrete foundation as well as where part of a column was embedded in the foundation with no stiffeners. A test programme was carried out with the aim of characterising these joints under monotonic, cyclic and random loads. Experimental results are presented by means of both force–interstory drift ratio and moment–rotation relationships. The outcomes demonstrated the adequacy of these joints to be used for MRFs of medium ductility class located in zones of moderate seismic hazard. Then, a numerical calibration of the whole joint subassemblies was successfully accomplished. Finally, non-linear time-history analyses performed on 2D MRFs provided useful information on the seismic behaviour of relevant MRFs. Copyright © 2015 John Wiley & Sons, Ltd.

Received 4 November 2013; Revised 4 December 2014; Accepted 10 December 2014

KEY WORDS: high-strength steel; beam-to-column joints; column-base joints; performance-based engineering; seismic behaviour; circular columns

1. INTRODUCTION

1.1. Background and motivation

High-strength steel is commonly employed in mechanical applications or in particular structural fields such as offshore structures and cranes where the requirement of strength is dominant in relationship to that of stiffness. In the last years, there has been a growing trend in the use of high-strength steel in tubular structures thanks to the publication of EN1993-1-12 [1] that extended the use of structural steel up to grades S690Q/S700MC. Nonetheless, EN1993-1-12 imposes many limitations at the level of material, structures and design owing to the limited knowledge of its actual behaviour. For instance, high-strength steel was found to be particularly advantageous for columns when the

*Correspondence to: Raffaele Pucinotti, Department PAU, Mediterranean University of Reggio Calabria, Reggio Calabria, Italy.

†E-mail: raffaele.pucinotti@unirc.it

horizontal displacement of the building is not a limiting condition or when columns are stocky [2]. Moreover, the use of high-strength steel can be advantageous in seismic design when employing the capacity design philosophy for non-dissipative elements owing to its inherent overstrength. Thus, columns in moment-resisting frames (MRFs) designed in high-strength steel and beams in mild steel can represent a convenient solution for structures located in moderate seismic prone zones when the limitation of lateral displacements is not dominant. A few papers have been published on the behaviour of high-strength steel employed in structural applications, and they are scattered on a wide range of topics: connections [3, 4], imperfections and residual stresses of very high strength steel circular tubes [5], circular hollow sections and concrete-filled tube (CFT) sections in fire [6] and strength of concrete-filled steel box columns [7, 8]. A Research Fund for Coal and Steel (RFCS) European research project called High-Strength Steel in Seismic Resistant Building Frames was funded with the aim of investigating and evaluating the seismic performance of dual-steel building frames made of mild steel and high-strength steel by employing I-sections or rectangular hollow sections, for example, refer to Silva *et al.* [9]. Nevertheless, there is a paucity of research addressed to the evaluation of the seismic behaviour of whole high-strength steel structural systems. Moreover, circular columns are suitable in structures subjected to loading in multiple directions because of uniform geometrical characteristics along all cross-sectional directions [10]; they constitute an inherent formwork when used as composite, and being a composite, they enhance fire resistance by allowing achieving the required performance level, for example, R90, without any fire protection [6]. Thus, their use is highly attractive and increasing also owing to its architectural and aesthetic properties, although still scarce. For this purpose, in order to promote the use of high-strength steel circular sections in buildings, the RFCS project called ATTEL was funded, with the aim of investigating both seismic and fire behaviour [11]. Objectives were set to deepen the knowledge at the level of as follows: (i) single structural elements made of high-strength steel, for example, moment–axial force interaction diagrams and section classification, and (ii) structural assemblies, such as joints, where the suitability of design formulae validated for mild steel grades was checked for high-strength steel. One main objective of ATTEL was the application of the performance-based engineering (PBE) technique [12] to a whole reference building made of high-strength steel taking into account the seismic interaction of different lateral-force-resisting systems in the two main directions: MRFs along one main direction and reinforced concrete (RC) shear walls along the other. In fact, only a few traces of analogous studies were found in literature [13] because probabilistic PBE analyses have been basically applied to 2D steel frames [14–16]. In order to provide a reliable representation of a probabilistic seismic demand model of these structural typologies, an accurate knowledge of their non-linear cyclic behaviour of the main critical components designed for withstanding lateral forces is needed. Nonetheless, because ground motion variability is more significant than uncertainties of structural parameters in affecting local engineering demand parameters, refer to, for instance, the results for a RC building [17], the aforementioned hysteretic representation will be deterministic. With regard to RC shear wall structures, their seismic response has already been extensively analysed; refer to among others [18–21]. Conversely and with reference to high-strength steel MRFs, it was deemed necessary to investigate new typologies of both beam-to-column (BTC) and column-base (CB) joints. The main goal of this paper is the presentation of the experimental results of such novel BTC and CB joints and of the analysis of their suitability to be used in medium ductility class (DCM) MRFs, whereas the results of the probabilistic seismic demand analysis on the 3D whole structure that exploits experimental data will be shown in future work.

1.2. Scope

The seismic behaviour of the aforementioned joint typologies together with the non-linear response of 2D high-strength steel MRFs represents basic aspects of a probabilistic seismic demand model and is the subject that this work explores further. Clearly, the design of both hollow elements and joints is directly correlated to fire action; in order to reduce complexity, fire actions are omitted herein based on the assumption that earthquake and fire are independent. Information on BTC joint behaviour under earthquake-induced fire can be found, for instance, in Pucinotti *et al.* [22].

In this view, the paper is organised as follows: Initially, Section 2 introduces design objectives of both reference structure and joints, whilst the experimental programme relative to both BTC joints and circular CBs is described in Section 3. Successively, relevant experimental results are discussed in Section 4. Furthermore, Section 5 presents finite element (FE) model calibration of all tested joint typologies and reports on the outcome of non-linear dynamic time-history analyses performed on MRFs. Finally, in Section 6, main conclusions are drawn with future perspectives.

2. DESIGN OF THE REFERENCE STRUCTURE AND OF JOINTS

In order to check the benefit of high-strength steel, a reference steel-concrete composite structure, depicted in Figure 1, was conceived as a case study with the objective of proposing structural elements and realistic configurations of BTC and CB joints to be tested in a laboratory. Therefore, a likely business building was considered. In order to better satisfy design criteria for static, seismic

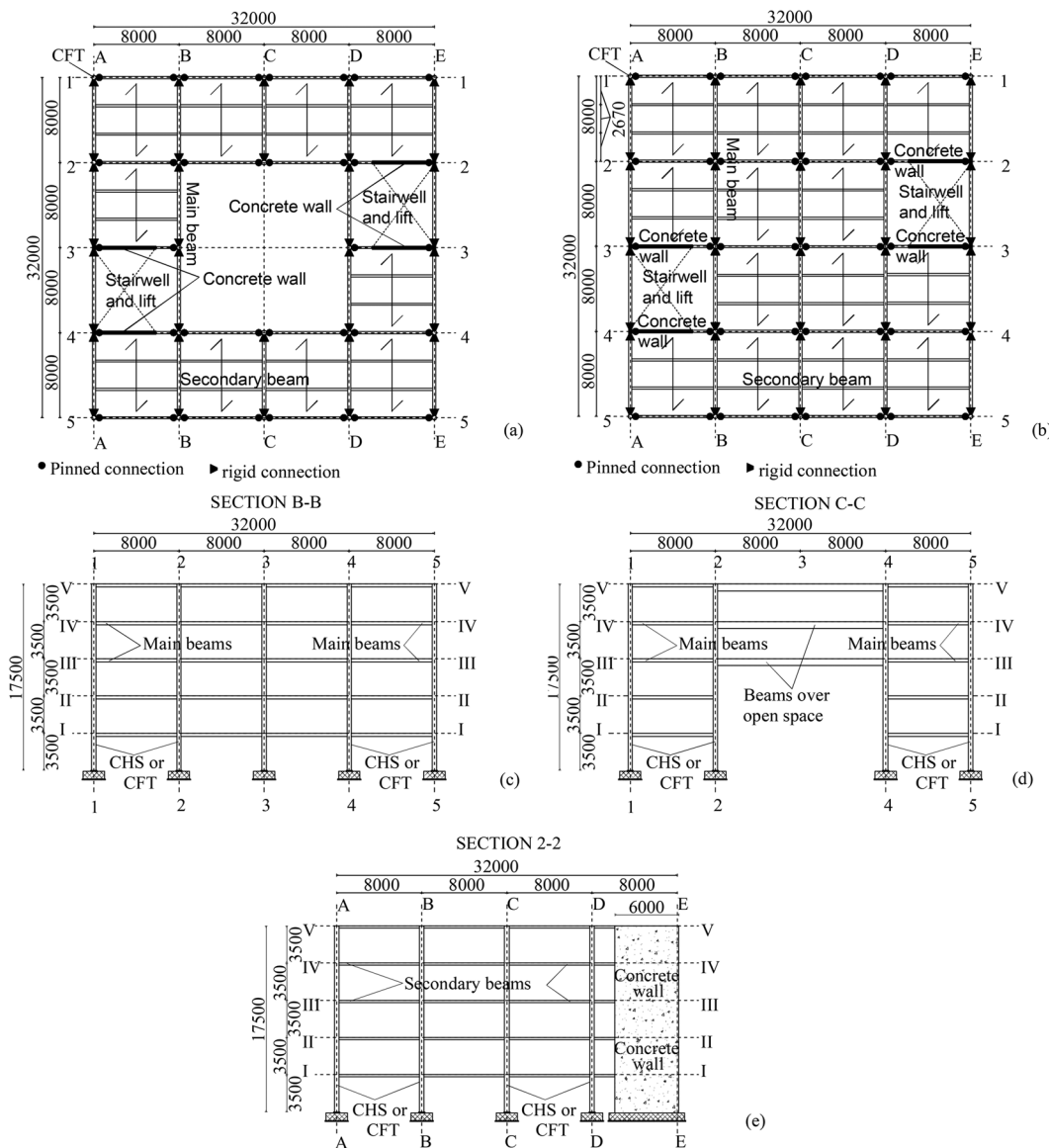


Figure 1. Reference structure: (a) plan of first and second floors; (b) plan of third, fourth and fifth floors; (c) B-B cross section; (d) C-C cross section and (e) 2-2 cross section. Dimensions in mm.

and fire loadings, MRFs along one main direction were designed, as shown both in Figure 1(c) and in Figure 1(d), whereas a steel pinned system was preferred in the other main direction by inserting RC shear walls, as illustrated in Figure 1(e). The choice of two different systems for withstanding lateral forces allowed for the optimisation of structural performance by avoiding MRFs in both principal directions: They could entail too severe column and joint designs.

The main features of the reference structure are the following: The plan dimensions are 32×32 m, and a central open space 16×16 m was created for the first three storeys, as shown in Figure 1(a) and (d); the structure was made up of five (4+1) MRFs placed at the distance of 8 m in one direction and of four RC walls (0.3×6 m) along the other direction. Moreover, two staircases, necessary to evacuate the building during fire, were located between the concrete walls. The interstorey height was 3.5 m. The main seismic design parameters of the reference structure were as follows: (i) DCM in agreement with EN1998-1 [23]; (ii) peak ground acceleration (PGA) a_g equal to $0.27 g$ corresponding to a moderate–high seismic action in Europe.

2.1. Moment-resisting frame design

As already mentioned, when employing MRF with columns made of high-strength steel in moderate-high seismic prone zones, stiffness requirements may become the limiting condition. Therefore, the damage limit state design in accordance with EN1998-1 [23] corresponding to an operational performance level in PBE design played a fundamental role in the seismic design of the reference structure being the requirement that governed the design. The ultimate limit state corresponding to a life safety performance level was also satisfied. The behaviour factor q was derived from a DCM penalised for irregularity in elevation owing to the presence of the open space; hence, $q=4\times 0.8=3.2$ [23]. Several MRFs with different geometric and material characteristics were designed in order to find the solution that could better exploit the qualities of high-strength steel. It resulted that the reference building with columns made of CFTs of steel grade S590 and composite beams of S275 steel grade represented the best frame assembly for withstanding static, seismic and fire loadings. Although high-strength steel was more expensive than mild steel of about 25% [24] in this particular case, relevant weight savings of steel columns entailed overall cost savings of about 5%. In detail, the composite beams were composed of S275 HEB 280 steel profiles fully connected to a C30/37 concrete slab 110 mm thick by means of Nelson 19-mm stud connectors whose height, spacing and ultimate tensile strength f_u were 100 mm, 140 mm and 450 MPa respectively. The thickness of the solid part of the concrete slab above the steel sheeting resulted adequate to serve as a rigid diaphragm. In fact, the slab exhibited less than 10% increase in horizontal displacements under seismic design actions when modelled with its in-plane cracked stiffness with respect to the assumption of a rigid diaphragm [23]. Structural profiled steel sheeting was used as illustrated in Figure 2(a). B450C steel grade was adopted for 3+3Φ12 additional longitudinal reinforcing steel bars that were arranged in such a way to satisfy the recommendations proposed in EN1998-1 [23] for the design of slabs of steel-concrete composite beams at BTC joints in MRFs. Circular columns of diameter 355.6 mm and thickness 12 mm were made of S590 high-strength steel and filled with concrete C30/37 and with a reinforcement cage composed of 8 Φ18 longitudinal bars and Φ8 at 150-mm stirrups, as shown in Figure 2(b). With these characteristics, the reference structure designed according to capacity design criteria withstood a seismic demand associated to a type 1

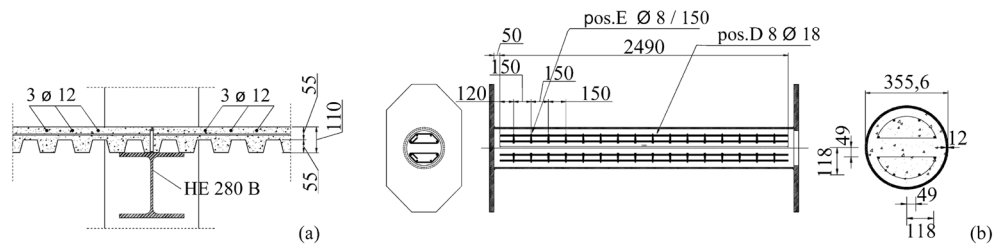


Figure 2. (a) Beam cross section and (b) CFT high-strength steel column. Dimensions in mm if not otherwise specified.

soil C elastic response spectrum with $PGA = 0.27 g$ in accordance with EN1998-1 [23], which as desired corresponds to a medium seismicity. Finally, the reference frame fulfilled the ‘damage limitation requirement’ of EN1998-1 [23] considering a drift limit of $0.01h$, where h is the storey height.

2.2. Joint design

2.2.1. Beam-to-column joints. The connection between an I-beam section and a circular CFT column entails an inherent higher complexity if compared with common BTC joints made of I-shape sections. Moreover, significant differences in the connection behaviour may occur depending on the load transfer path from the beam to the column. In fact, analytical studies suggested that connections that transfer load from the girder to the concrete core, for example, through-in steel plates, potentially offer better seismic performance by exhibiting enhanced strength and stiffness characteristics than connections that apply the load to the steel tube alone. Indeed, the latter solution may exhibit large distortion of the tube wall around the connection region [25]. A through-in plate, Figure 3(b), consists of a vertical plate that passes through the tubular column at the level of the joint, typically of the same thickness of the beam web. Such a solution is very convenient when having an H-beam section because the beam web can be directly and easily connected to the through-in plate by means of cover plates. In addition, according to the capacity design philosophy, the collapse mechanism shall avoid the formation of plastic hinges in columns; thus, columns shall exhibit enough overstrength with respect to adjacent beams. Finally, based on these considerations, it was decided to add a vertical through-in steel plate in the column concrete core.

The proposed welded/bolted solution was conceived in order to guarantee ease of assembly and limited problems related to on-site welding [26]. The seismic design of the composite BTC joint, depicted in Figure 3, was devised to provide the non-dissipative components, that is, columns, with adequate overstrength and stiffness with respect to the dissipative connected members, that is, cover plates of the connection.

In detail, according to the seismic design of the reference frame shown in Figure 1(c), BTC joints were assembled by means of horizontal and vertical S355 plates welded to the column and bolted to beams by means of M20 and M27 Class 10.9 preloaded bolts. The joint was designed to be

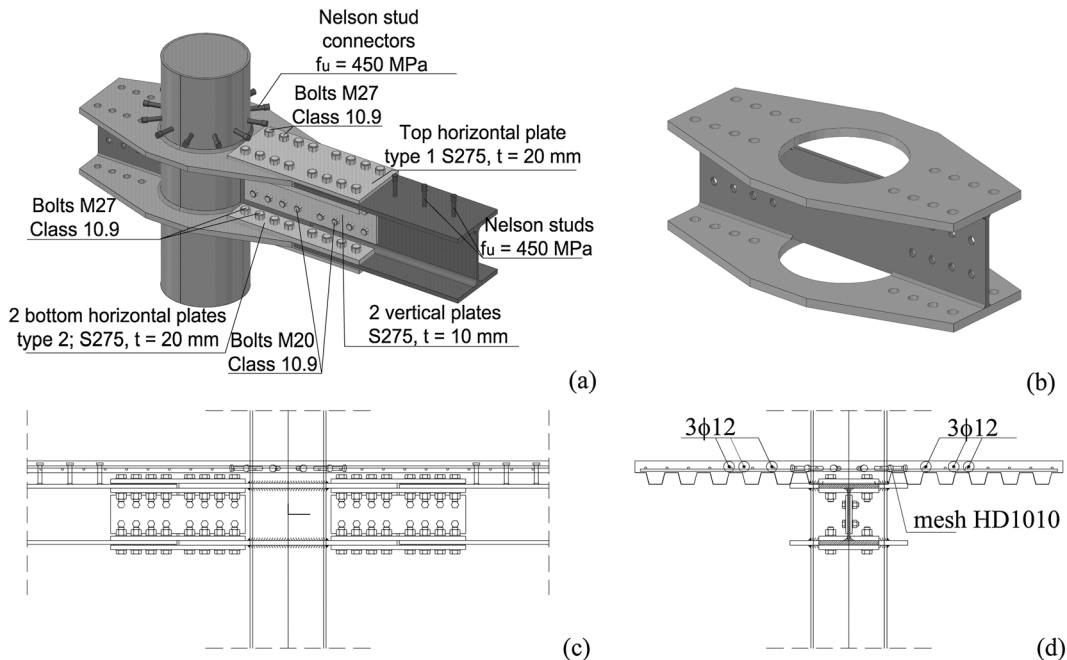


Figure 3. Beam-to-column joint, (a) 3D view, (b) detail of the vertical through-in plate, (c) lateral view and (d) cross section.

Category B—slip resistant at serviceability limit state—in agreement with 1993-1-8 [27]. In order to directly transfer shear to the concrete core, a vertical steel plate—of thickness 10 mm and of the same height of the steel beam web—passing through the column was provided. Then, in order to enable the development of the seismic slab-to-column transfer mechanism, an additional steel mesh $\Phi 10$ at 100×100 mm was placed in the slab [23]. In fact, a steel mesh was needed to activate Strut and Tie Mechanisms 1 and 2 as foreseen in EN1998-1 [23] and detailed in Pucinotti *et al.* [26]. Differently from Pucinotti *et al.* [26], Nelson stud connectors were interrupted close to the joints, as shown in Figure 3. This choice was recommended by the steel workshop and was adopted both to reduce time for shop operations and to facilitate joint erection. Conversely, horizontal connectors welded around the column at the slab level were left in place. In a capacity design perspective, fillet welds on the column were overmatching, that is, of higher strength with respect to S355 steel plates. The BTC joints were designed according to the component method [27]. Because EN1993-1-8 [27] does not provide formulae for some components, especially for tubes, the concrete slab in compression and the top horizontal plate in tension were characterised by means of FE models suggested in Pucinotti *et al.* [26].

2.2.2. Column-base joints. With reference to CB joints, two different solutions both rigid and full strength were designed: (i) a standard solution with a base plate, anchor bolts and vertical stiffeners, as shown in Figure 4(a), and (ii) an innovative solution with the column embedded in the foundation, as illustrated in Figure 4(b), respectively. The latter is surely better suited for CFT columns because of an increase in strength owing to the tube embedded in the foundation as well as improved ease of construction that does not entail stiffeners welded to the base plate. Both solutions were designed to meet capacity design criteria. The standard joint was designed according to EN1998-1 [23], and the effects of actions on foundation elements were derived on the basis of capacity design considerations accounting for development of possible overstrengths.

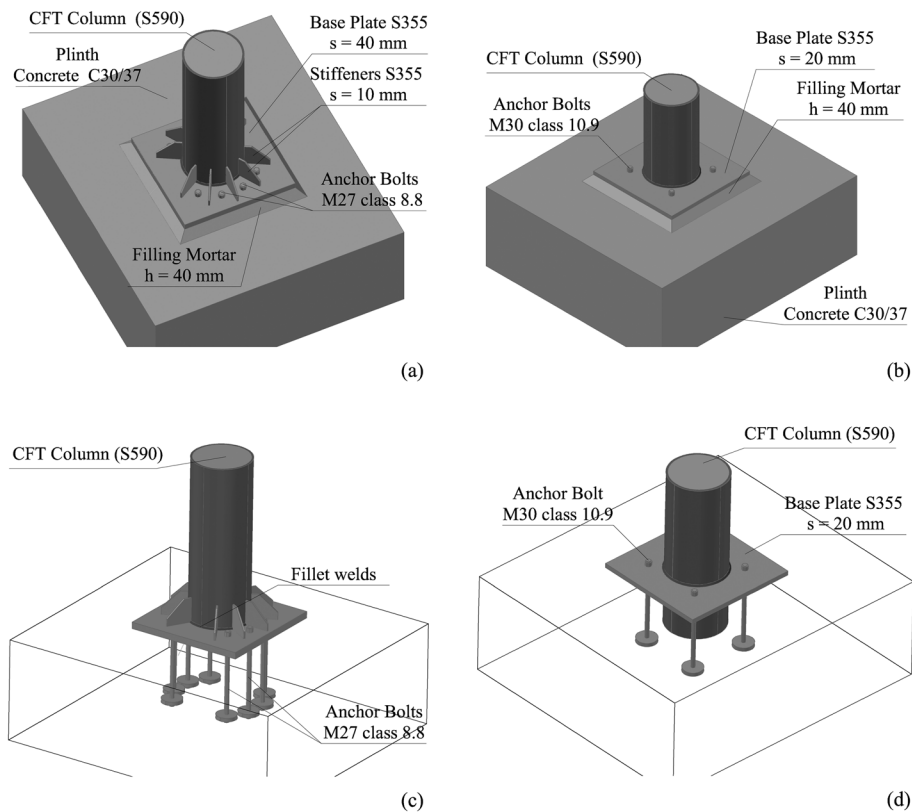


Figure 4. Column-base joints: (a) standard solution and (b) innovative solution.

The innovative CB joint was designed according to Strut and Tie mechanisms devised for prefabricated concrete structures according to EN1992-1-1 [28], where forces and moments can be transferred from a column to a foundation by compressive forces through the concrete filling. It is important to emphasise that the formulae proposed in EN1992-1-1 [28] for pocket foundations refer to rectangular columns embedded in the plinth. Therefore, it was deemed necessary to investigate whether the Strut and Tie mechanisms conceived to transfer forces between column and foundation could actually develop. Consequently, a 3D numerical model of the innovative CB joint was implemented by using the ABAQUS software [29]. Figure 5 shows the results of the numerical analysis that well agree with the design assumptions.

In detail, 8M27 class 8.8 anchor bolts were employed in the standard joint, whilst 4M27 class 8.8 anchor bolts were adopted in the innovative joint with the only function to ease the column erection. The class of foundation concrete was C30/37, and all rebars were of steel grade B450C.

3. EXPERIMENTAL CAMPAIGN

3.1. Tests on materials

Before testing the full-scale specimens, an extensive characterisation of material properties was carried out. This was performed on structural steel and reinforcing steel because concrete was tested on the day of each test. The aim was twofold: (i) to estimate the actual strength of the specimens in order to design all components of the set-up and (ii) to obtain actual material properties to be used in numerical modelling.

3.1.1. Structural steel. Table I reports on the average values of yield strength f_y , ultimate strength f_u and elongation of the plates used for the connection between columns and beams. The reported values were obtained by means of tensile tests performed in accordance with ISO 6892-1 [30]. A steel grade S590QL was requested for each column. Nonetheless, tests showed average values of yield strength and ultimate strength of about 690 and 766 MPa respectively, with elongations greater than 19%.

Although these properties satisfied quality control of the steelwork supplier, we understood that steel mills tend to use high-strength steel for specific applications, for example, tower cranes made of CHS

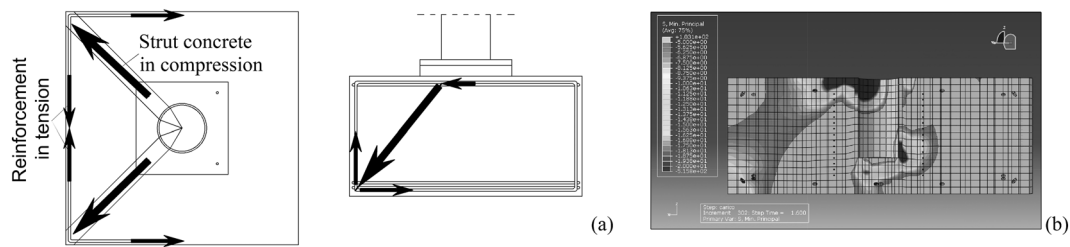


Figure 5. Innovative column-base joint: (a) Strut and Tie transfer mechanism in the foundation and (b) distribution of stresses in the 3D FE model.

Table I. Average material properties of structural steel.

Element	Steel	t (mm)	f_y (MPa)	f_u (MPa)	Elongation (%)
Plate	S355JR	10	404	543	28
Plate	S355JR	12	398	556	27
Plate	S355JR	25	396	545	29
Plate	S355JR	40	391	566	30
Plate	S355JR	45	394	517	25
Plate	S275JR	20	308	443	34
Plate	S275JR	10	315	441	35
CHS355.6	S590QL	12	690	766	19
HEB280	S275JR	—	307	462	33

with steel grade higher than S690, and therefore, also, their adaptation to different grades requires accurate analysis and enough casts to optimise the product. The other values complied with the specifications provided in EN10025-2 [31]. Thus, overstrength criteria required by EN1998-1 [23] and envisaged in the design process were actually satisfied.

3.1.2. Concrete. Table II reports on the average values R_{cm} of the cubic compressive strength of concrete used for the CB foundation, the filling of columns used in BTC joints and in CB joints, and the slab.

3.1.3. Steel reinforcements. Tensile tests on the steel reinforcement used in the specimens led to average yield strength of about $f_y = 540 \text{ MPa}$, ultimate strength of $f_u = 640 \text{ MPa}$ and an elongation $A_{gt} > 7.5\%$.

3.2. Test programme

In order to understand both the global and the hysteretic behaviour of BTC joints and CB joints, as well as the activation of mechanisms in critical parts, seven tests on full-scale subassemblies were performed by applying cyclic and monotonic test protocols.

In detail, the following test programme was conceived: (i) a monotonic test in order to estimate both maximum force level and maximum rotational capacity of the BTC joint described in Subsection 2.2.1 as well as to check the position of plastic hinges; (ii) cyclic tests according to the ECCS procedure [32], modified according to SAC provisions [33], in order to evaluate the hysteretic behaviour of a joint in terms of strength and stiffness degradation and in terms of rotational capacity under cyclic loading; and (iii) random tests in order to characterise the actual behaviour and performance of a joint under seismic loading. The complete test programme is summarised in Table III, whilst the cyclic loading protocols are shown in Figure 6.

Joint tests were carried out in displacement control. The maximum displacement imposed in the monotonic test was about 240 mm. The benchmark displacement e_y imposed to the specimens tested according to ECCS procedure [32] was evaluated, in agreement with the SAC provisions [33] as $e_y = \Theta h$, by assuming an interstorey drift angle Θ of 5 mrad [33], where h is the storey height. It is worth to point out that the storey height for BTC specimens is 3.5 m, whereas for CB specimens, it corresponds to $h = 1.75 \text{ m}$.

The random tests were performed using as an input the interstorey drift provided by the non-linear structural analysis of the 2D frame subjected to seismic loading by means of a far-field spectrum-compatible accelerogram, in agreement with EN1998-1 [23]. In order to obtain displacements in the

Table II. Concrete strength properties.

Element	Concrete strength class	R_{cm} (MPa)
Column-base joint	C30/37	48.2
Filling of columns—CB joints	C30/37	50.4
Filling of columns—BTC joints	C30/37	48.7
Slab	C30/37	48.7

Table III. Test programme.

Number	Label	Test protocol	Type of specimen
1	BTCJM	MONOTONIC	BTC joint
3	BTCJE	ECCS-SAC	BTC joint
2	BTCJR	RANDOM	BTC joint
4	CBJSEE	ECCS-SAC	Standard CB joint
5	CBJSER	RANDOM	Standard CB joint
6	CBJINE	ECCS-SAC	Innovative CB joint
7	CBJINR	RANDOM	Innovative CB joint

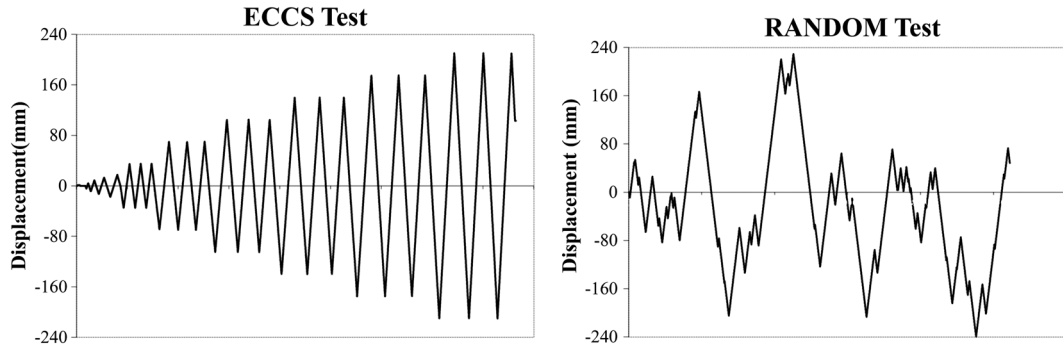


Figure 6. Cyclic loading protocols.

loading protocol comparable to those recorded during the ECCS test, the value of the PGA was then increased up to about 1.8 g.

3.3. Test set-up

The lengths of columns and beams in each joint solution were decided so as to be in correspondence to inflexion points, that is, points of zero bending moment. In this way, it was possible to simplify the load application and the whole set-up.

Therefore, a system of trusses and of hinge restraints was employed, as shown in Figures 7 and 8 respectively. Loads were applied by means of a hydraulic actuator that was attached

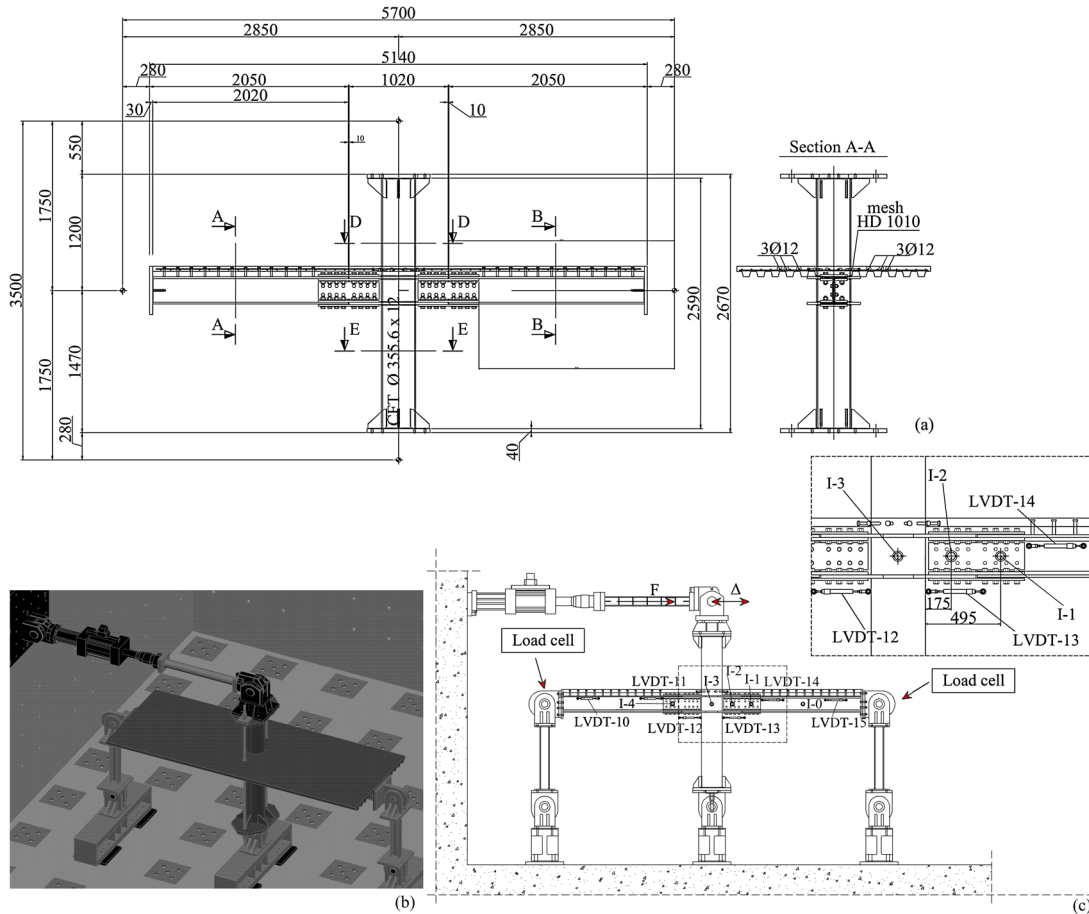


Figure 7. BTC joint: (a) BTC specimen, (b) test set-up and (c) instrumentation. Dimensions in mm.

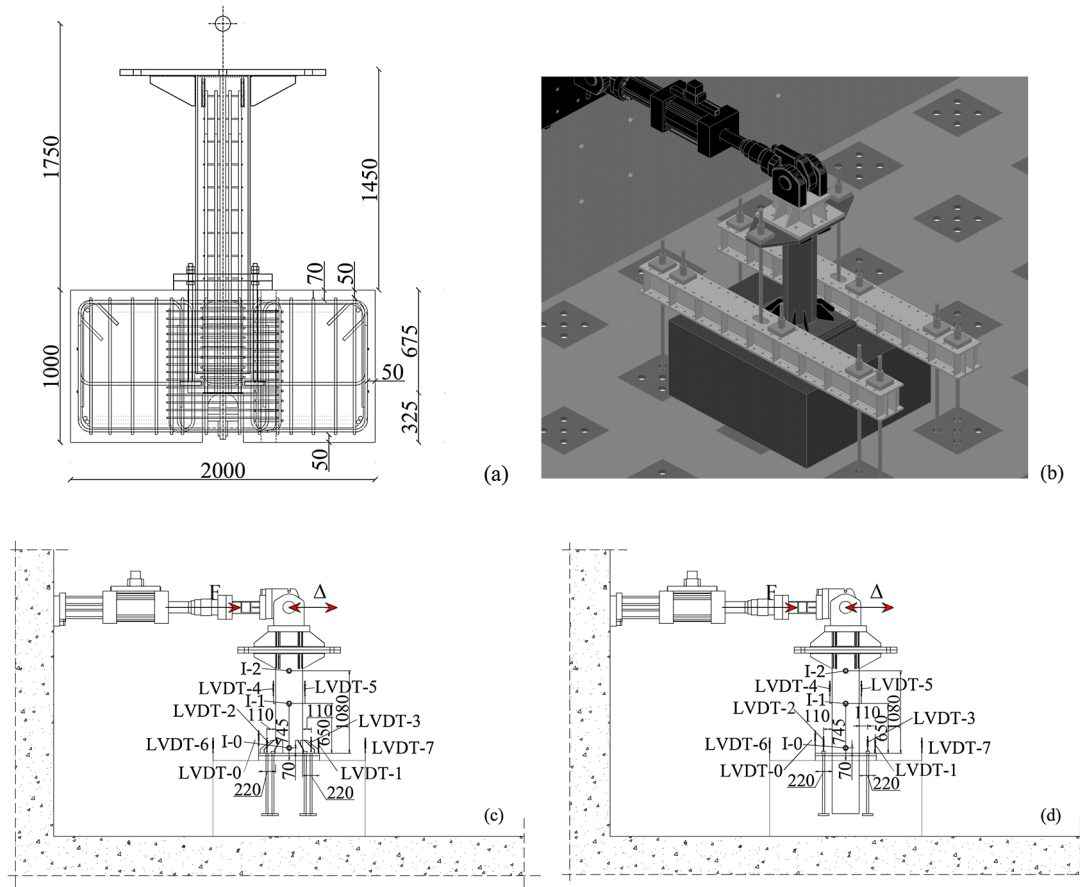


Figure 8. CB joint: (a) reinforcing bar arrangement of the innovative solution, (b) test set-up, (c) instrumentation on standard joints and (d) instrumentation on innovative joints. Dimensions in mm.

horizontally to the reaction wall of the Laboratory for Material and Structural Testing of the University of Trento. The actuator was displacement controlled. In order to be consistent with the static loads applied to the reference frame, during the tests, a vertical constant load of about 700 kN was imposed by means of Dywidag bars at the top column of the BTC joints and 700 kN at the top of the CB joints, as shown in Figures 7(b) and 8(b) respectively. Vertical forces were not controlled; however, they were either checked at the beginning of the test—for BTC joint tests—or initially checked and thoroughly monitored during the whole duration of the tests—for CB joint tests. In CB joint tests, the vertical load increased about 20% from initial to ultimate conditions. A comprehensive instrumentation set-up was provided in order to measure deformations, displacements, rotations and forces of the various components that compose the joints.

The main instruments used and depicted in Figures 7(c) and 8(c) and (d) were as follows:

- (1) inclinometers used to monitor the flexural deformation of the joint,
- (2) linear variable differential transformer (LVDT) displacement transducers adopted to monitor the elongation of the joint components,
- (3) LVDTs used to detect possible interface slip between the steel beam and the concrete slab,
- (4) strain gauges adopted to monitor strains of plates, of flanges and of reinforcing bars,
- (5) load cells used to measure horizontal and vertical components of the applied forces, and
- (6) omega-shaped strain gauges used to monitor deformations of the concrete slab around the column in BTC joints.

4. TEST RESULTS

4.1. Beam-to-column joints

The force–interstorey drift ratio and moment–rotation relationships of BTC joints are depicted in Figure 9.

The maximum displacement reached in the ECCS test was $\pm 12e_y$, equal to about ± 210 mm, close to the available stroke of the actuator. Focussing on the cyclic behaviour, both in the BTCJE test and in the BTCJR test, the hysteretic response was significantly favourable with high energy dissipation. Plastic hinges developed in the weak section between the plates welded to the column and the beam end, as highlighted in Figure 10(a). Thus, the joint behaved as of partial strength. The rotation of the plastic hinge in BTC joints was determined as the difference between readings of inclinometers I-1 and I-2, shown in Figure 7(c). Inclinometers I-3 and I-2 were used to check the assumption of rigid behaviour. The progressive deterioration of strength and stiffness as well as the joint failure was mainly caused by concrete damage near the column, as shown in Figure 10(b). The moment–rotation relationship recorded in the ECCS test showed a sudden reduction of strength in the sagging moments, owing to degradation of concrete in compression.

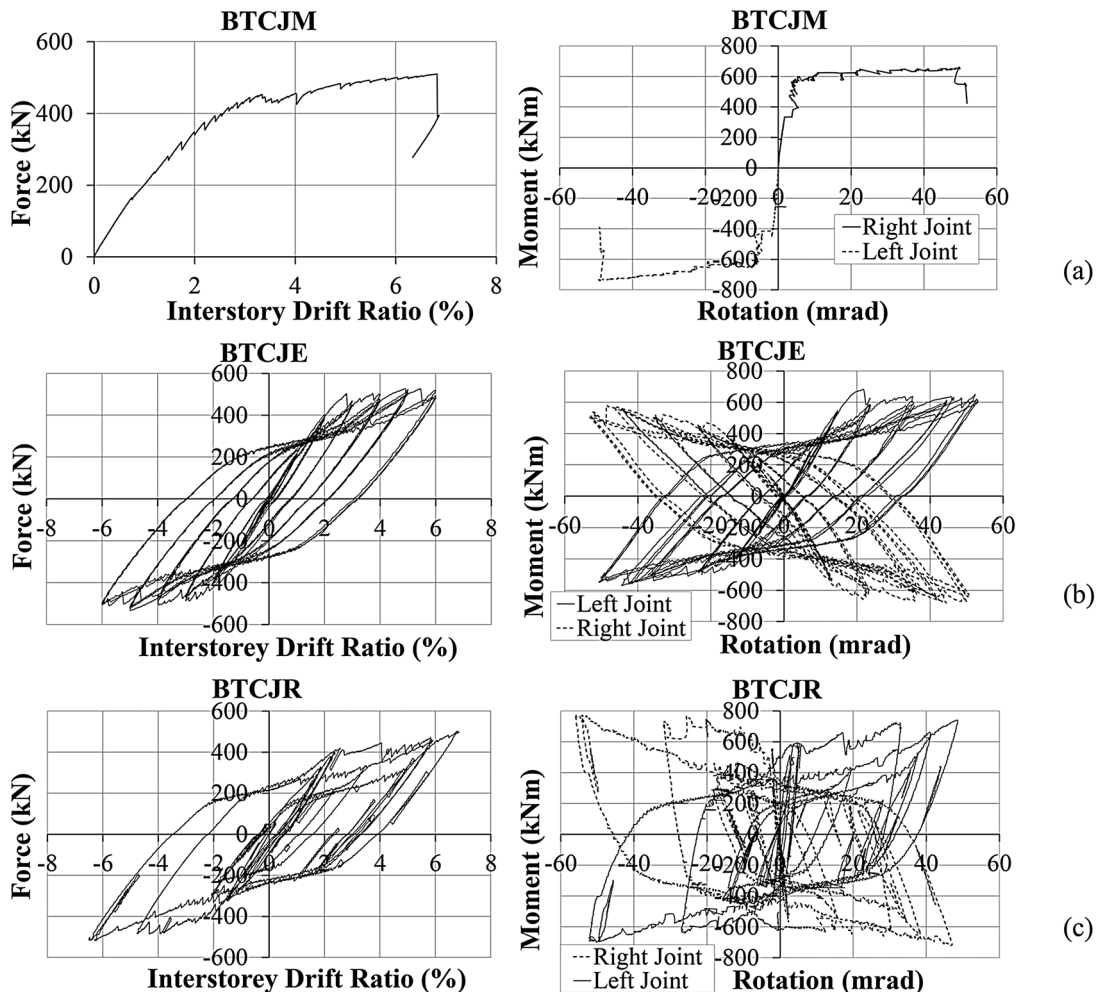


Figure 9. Force–interstorey drift ratio curves and moment–rotation relationships: (a) BTCJM, (b) BTCJE and (c) BTCJR.

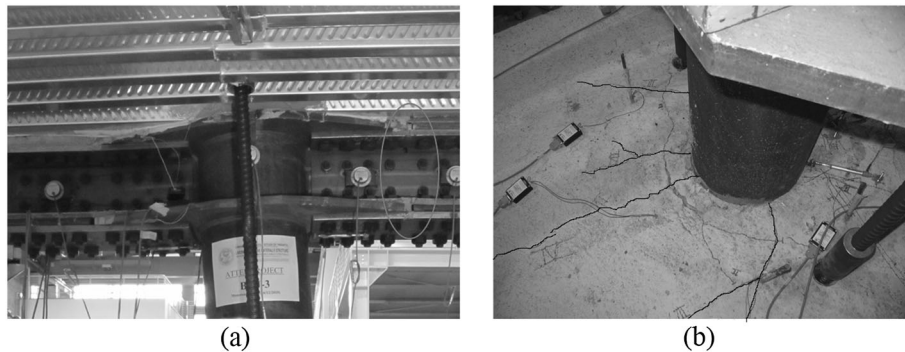


Figure 10. BTC specimen after the ECCS test: (a) position of the plastic hinge and (b) damage in concrete slab.

The absence of Nelson stud connectors on the upper cover plates, as a result of practical workshop needs, facilitated the concrete degradation near the column. Despite the damage of the slab, the BTC joint exhibited a favourable hysteretic behaviour. The Strut and Tie mechanism envisaged in the EN1998-1 [23] clearly developed on the concrete slab as observed in Figure 10(b). Moreover, specimens subjected to cyclic and random loadings developed plastic rotations much greater than 25 mrad, that is, 40 mrad, without significant stiffness and strength degradation, thus being adequate for MRFs of DCM [23]. Stiffness degradation in BTC and CB joints was determined by comparing the initial stiffness value with the slope at each unloading branch corresponding to zero load conditions: It was never found to be more than 20%. Strength degradation was determined by comparing the overall maximum strength exhibited by the joint with the maximum strength reached at subsequent cycles: It was never more than 20%. The moment–rotation relationships highlighted several important aspects of the behaviour of the examined joint. One aspect was slippage at high levels of displacements owing to hole clearance in agreement with the design of the joint that belonged to Category B [27]. Slippage occurred between the cover plates and the plates welded at the column as well as between the cover plates and the beam. Another relevant aspect was the high value of rotation without significant stiffness and strength degradation; this is very interesting for the hogging moment regime because similar joints often exhibit significant degradation caused by instability of bottom flanges and webs in compression [26]. For the joint under exam and owing to slippage, the plastic hinge developed in the aforementioned weak section, and it did not involve beam sections outside cover plates; this is the reason why no flange buckling was observed when subjected to hogging moment.

4.2. Column-base joints

With regard to the standard seismic joints subject to cyclic (CBJSEE) and random (CBJSER) loadings, the experimental results are depicted in Figure 11(a) and (b) respectively.

In this case, the CB joints were pushed up to a displacement of $\pm 16e_y$, equal to about ± 140 mm. Both force–interstorey drift ratio relationships and moment–rotation curves exhibited a hysteretic behaviour characterised by large energy dissipation without evident loss of resistance and stiffness before collapse. In fact, the response of the standard CB joints under cyclic loading was characterised by ductile behaviour without significant stiffness and strength degradation associated with plastic rotations of about 45 mrad, measured by means of inclinometer I-0, as illustrated in Figure 8(c) and (d). Failure of the joints was caused by anchor bolts in tension after the activation of the plastic hinge, as shown in Figure 12(b). The innovative seismic joints exhibited a similar cyclic response characterised by large plastic rotations but developed a greater resistance than standard seismic joints, as highlighted in Figure 11(c) and (d). The hysteretic behaviour was characterised by two plastic hinges: (i) One plastic hinge was located in the plinth because of compression on the concrete filling owing to column rotation and (ii) a second

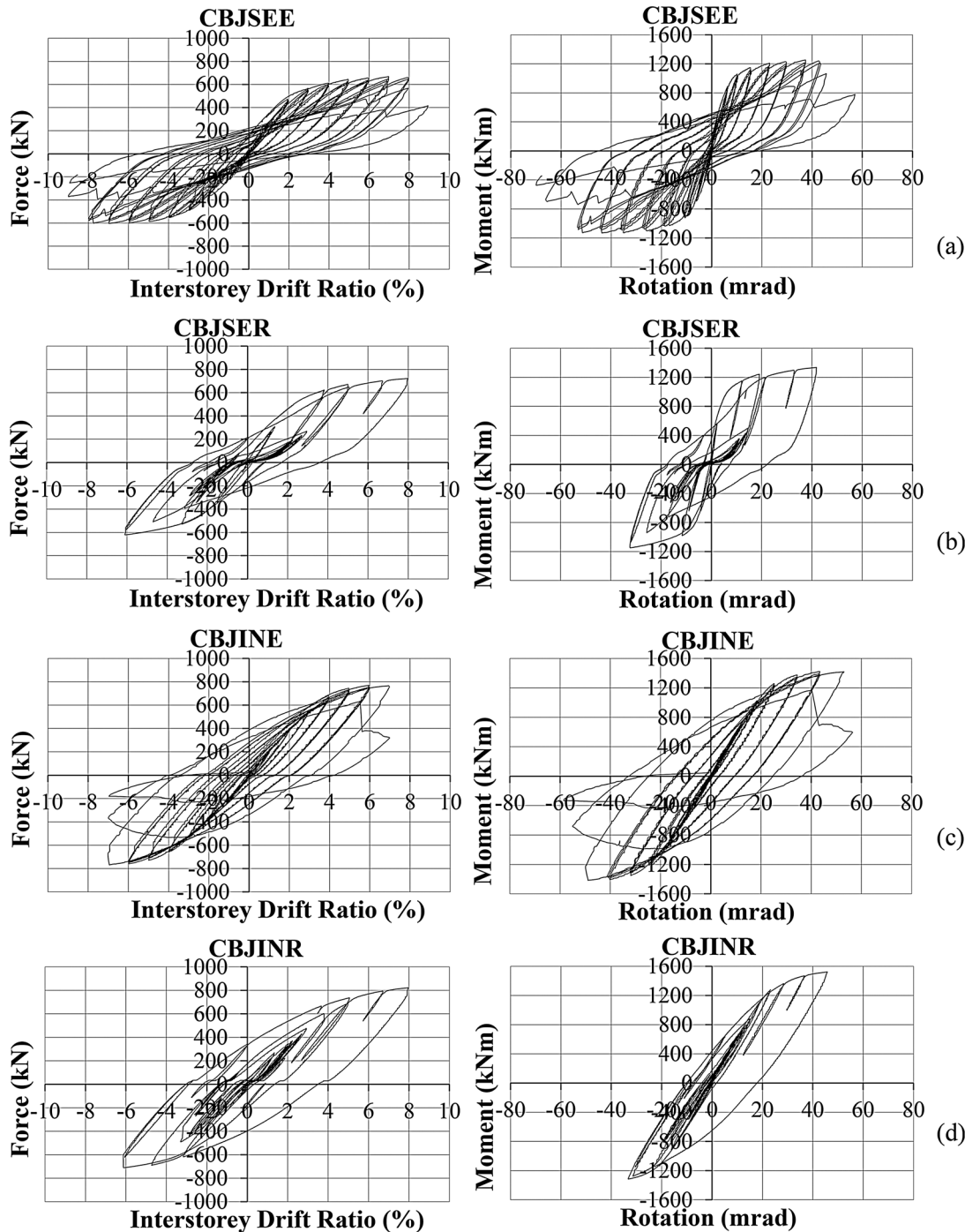


Figure 11. Force–interstorey drift ratio curves and moment–rotation relationships: (a) CBJSEE, (b) CBJSER, (c) CBJINE and (d) CBJINR.

plastic hinge located on the column outside the plinth detected by computing the difference between I-1 and I-0 (Figure 8(c) and (d)). Collapse was caused by brittle failure of the column wall near the weld between the column and the base plate owing to phenomenon of local instability in the wall of the column, as depicted in Figure 12(d). In this case, plastic rotations exceeded 45 mrad. Finally, with reference to CB joints, no requirements of a minimum plastic rotation are provided in EN1998-1 [23].

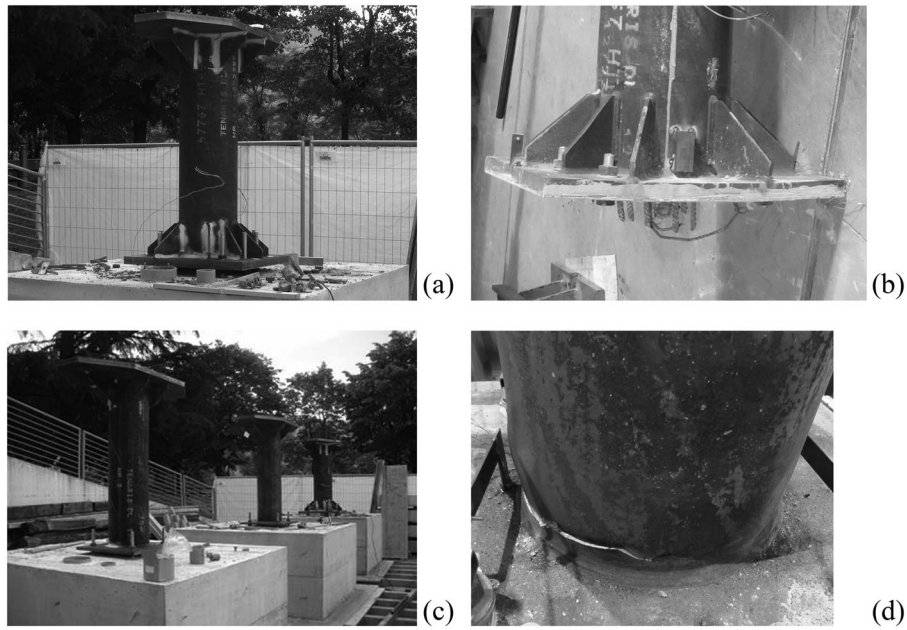


Figure 12. Failure modes of CB joints: (a–b) CBJSEE joint and (c–d) CBJINE joint.

5. CALIBRATION OF JOINTS AND ANALYSIS OF THE SEISMIC BEHAVIOUR OF MRFS

As described in the Introduction, in order to reliably represent the probabilistic seismic demand model of the whole five-storey reference structure, an accurate modelling of the hysteretic behaviour of each component that withstands lateral forces is needed. For this reason, the calibration of the joints of the MRF and the relevant analysis of the seismic design assumptions based on joint calibration were performed.

5.1. Calibration of the joint assemblies

It is important to point out that the numerical calibration was performed on the whole joint subassemblies that were experimentally tested, as shown in Figure 13. Thus, a far more complex process occurred than the calibration of a single plastic hinge. In detail, the lumped plasticity approach was applied, and the numerical modelling was performed with the OpenSees software [34].

The material models that were used to represent the inelastic behaviour were a Bouc–Wen material model in parallel to a pinching hysteretic model. The Bouc–Wen model provided the main part of the actual inelastic behaviour, whereas the pinching model simulated slip owing to damaged concrete and

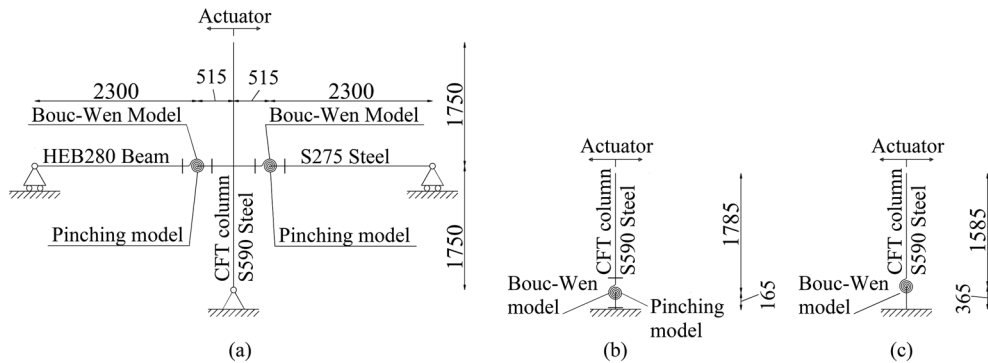


Figure 13. Numerical model of joints: (a) BTC, (b) standard CB and (c) innovative CB. Dimensions in mm.

consequent hardening; it also took into account the different behaviour between hogging and sagging moment, particularly in BTC joints.

As an exception, the calibration of the innovative CB joint was possible by only considering the Bouc–Wen model. More details about the hysteretic models are available in Appendix A. Figure 14 shows the comparison between experimental and numerical relationships in terms of force–interstorey drift ratio and moment–rotation of all the tested joints subjected to the ECCS loading protocol. In order to calibrate the model, a trial and error procedure was applied.

In particular, the values of model parameters were varied within their range of applicability with the aim of obtaining an optimal match between numerical and experimental results. In Table IV, the quantitative measure of dissipated energy, computed as the sum of areas underlying the moment–rotation curves, is compared. By taking into account the complexity of the joint assemblies, a good agreement between experimental and numerical outcomes may be observed.

5.2. Evaluation of the seismic behaviour of MRFs

In order to provide useful information on the seismic behaviour of MRFs made of such joint typologies and on how joint design translates into MRF performance, it was decided to apply the incremental dynamic analysis (IDA) method proposed by Vamvatsikos and Cornell [42]. With this objective in mind, two MRFs shown in Figure 15(a) and (b)—MRF-S endowed with calibrated standard CB

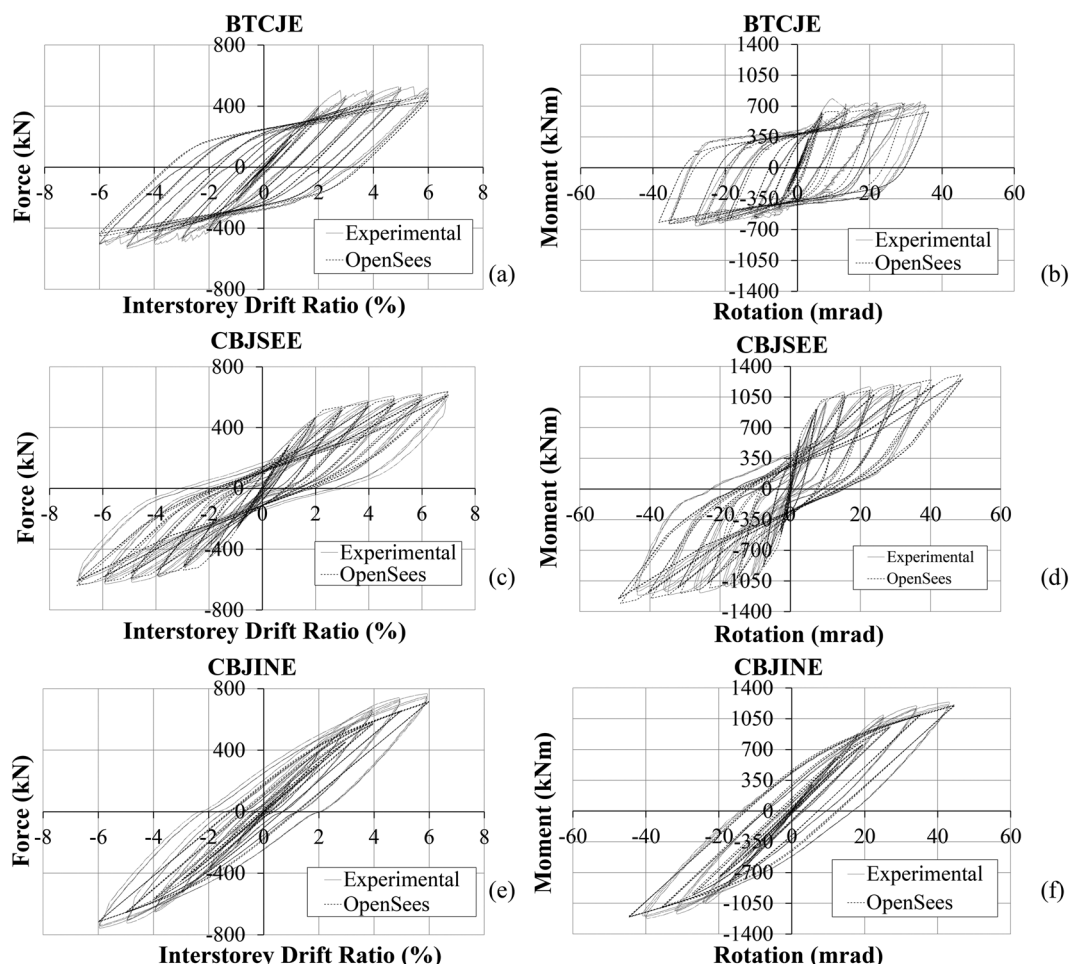


Figure 14. (a) BTCJE force–interstorey drift ratio comparison, (b) BTCJE moment–rotation comparison, (c) CBJSEE force–interstorey drift ratio comparison, (d) CBJSEE moment–rotation comparison, (e) CBJINE force–interstorey drift ratio comparison and (f) CBJINE moment–rotation comparison.

Table IV. Comparison of dissipated energy between experimental and numerical results.

Specimen	Test protocol	Experimental (kJ)	Numerical (kJ)	Error (%)
BTCJM	MONOTONIC	352.7	310.2	12.1
BTCSR	RANDOM	154.4	144.3	6.6
BTCE	ECCS-SAC	19.1	20.0	4.7
CBJSEE	ECCS-SAC	352	413	14.8
CBJSER	RANDOM	110	148	25.7
CBJINE	ECCS-SAC	275.9	245.2	12.5
CBJINR	RANDOM	83.3	112.1	25.7

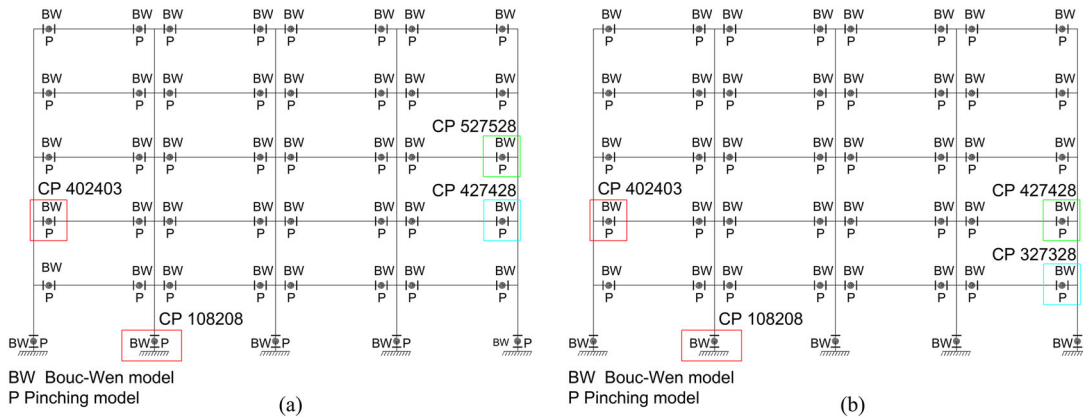


Figure 15. MRF FE models: (a) MRF-S with standard CB joints and (b) MRF-I with innovative CB.

joints and MRF-I with calibrated innovative CB joints—extracted from frame B-B of Figure 1a were modelled; calibrated BTC joints as described in Subsection 5.1 were included too. Note that strictly speaking, this 2D frame analysis may not be representative of the dynamic behaviour of the entire reference structure of Figure 1 because of elevation irregularity. A complete analysis of the seismic behaviour of the whole reference structure can be found in Sozonov *et al.* [35]. The tributary mass of each 2D frame storey was distributed along the primary beams. In particular, it was lumped at BTC intersections and in correspondence to the points where secondary beams connect to primary beams (Figure 1(a) and (b)).

A lumped plasticity model was exploited for the connections, whereas the other parts of the frame were modelled with linear-elastic-displacement-based beam-column elements as developed in Mazzoni *et al.* [34]. For beams, the flexural stiffness (EI) of such elastic elements was assigned constant along their length and based on the average between the flexural stiffness under sagging moment, that is, no slab cracking, and the flexural stiffness under hogging moment, that is, by allowing for slab cracking. For columns, the effective flexural stiffness was computed according to EN1994-1-1 [36].

Incremental dynamic analyses were performed for each frame on the basis of three spectrum-compatible artificially generated accelerograms; in particular, they matched type 1 elastic response spectrum of soil type C in accordance with EN1998-1 [23]. Significant PGA levels corresponding to as follows: (i) First yielding of a BTC joint, that is, pga_y ; (ii) plastic rotation of 25 mrad, that is, $pga_{(25 \text{ mrad})}$; and (iii) near collapse, that is, pga_u , are gathered in Table V for both MRF-S and MRF-I. Note that the near-collapse condition corresponded to a conventional interstorey drift ratio value of 5%, taken from FEMA 356/2000 [37] and assumed as a structural performance index in terms of deformability.

Moreover, at near collapse, both BTC joints and CB joints never suffered either stiffness or strength degradation greater than 20% because rotation demands were within the range in which degradation was not observed in the experiments, thus complying with general joint requirements established by EN1998-1. One careful reader can observe that BTC joints approach a limit value of 25 mrad for

Table V. Seismic response parameters from IDAs.

Frame	MRF-S			MRF-I		
	1	2	3	1	2	3
Accelerogram						
a_g (g)	0.27	0.27	0.27	0.27	0.27	0.27
pga_y (g)	0.64	0.33	0.58	0.56	0.33	0.56
$pga_{(25 \text{ mrad})}$ (g)	1.75	1.43	1.98	1.68	1.33	1.80
pga_u (g)	2.30	1.75	2.25	2.30	1.57	2.20
q_{dyn}	3.62	5.38	3.88	4.11	4.76	3.93
Ω_{dyn}	7.53	3.85	6.87	6.64	3.91	6.64
$q_{dyn} \cdot \Omega_{dyn}$	27.26	20.71	26.66	27.29	18.61	26.10

$pga_{(25 \text{ mrad})}$ values much greater than the design a_g value; therefore, they satisfy EN1998-1 requirements, mentioned in Subsection 4.1, for their use in MRFs of DCM. Relevant relationships are depicted in Figures 16(b) and 17(b) for MRF-S and MRF-I respectively; for completeness, also relationships corresponding to pga_y and pga_u are represented in the same figures. With regard to CB joints, IDAs showed that CB approach values of -36.0 and -41.3 mrad for MRF-S and MRF-I respectively. The comparison between these values and the ones exhibited by specimens, Sub section 4.2, draws to the conclusion that also these joints are compatible with MRFs of DCM. Dynamic response curves provided by IDAs allowed for the definition of both the dynamic behaviour factor q_{dyn} —where dynamic stands for a behaviour factor obtained from dynamic analyses—and the overstrength factor Ω_{dyn} according to Bursi *et al.* [38].

In greater detail,

$$q_{dyn} = \frac{pga_u}{pga_y}; \quad \Omega_{dyn} = \frac{pga_y}{pgad}; \quad pgad = \frac{a_g}{q} \quad (1)$$

with $q=3.20$ as for the reference structure. The values of $q_{dyn} \cdot \Omega_{dyn}$ reported in Table V are much higher than the design q value of the reference structure and much higher than any design q values provided for steel frame structures in EN1998-1 [23], owing to both high q_{dyn} —which accounts for

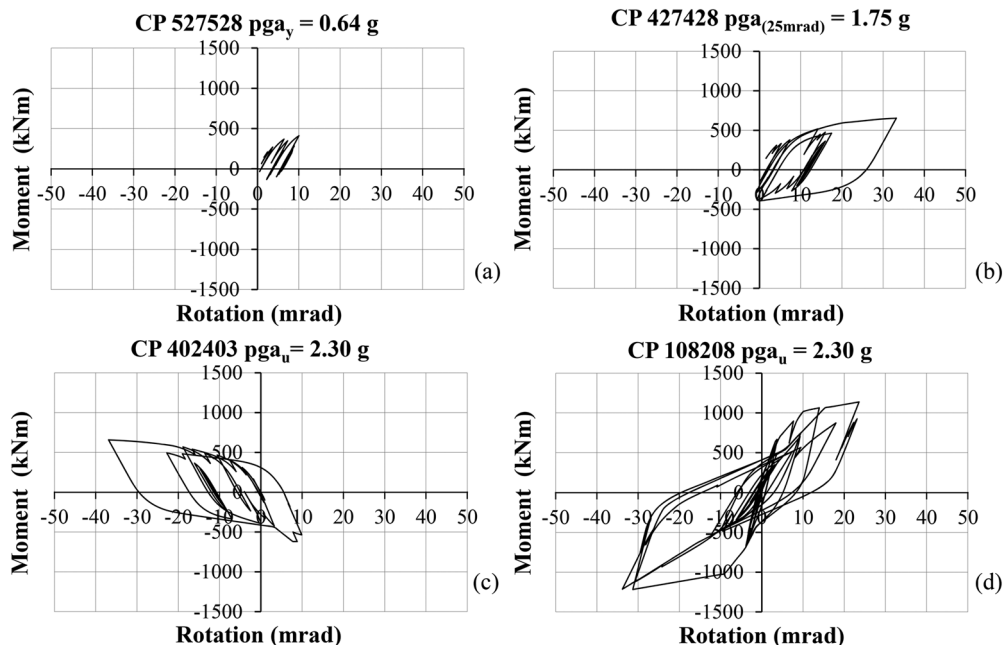


Figure 16. Moment–rotation relationships for MRF-S owing to accelerogram 1 of (a) BTC joint at pga_y , (b) BTC joint at $pga_{(25 \text{ mrad})}$, (c) BTC joint at pga_u and (d) CB at pga_u .

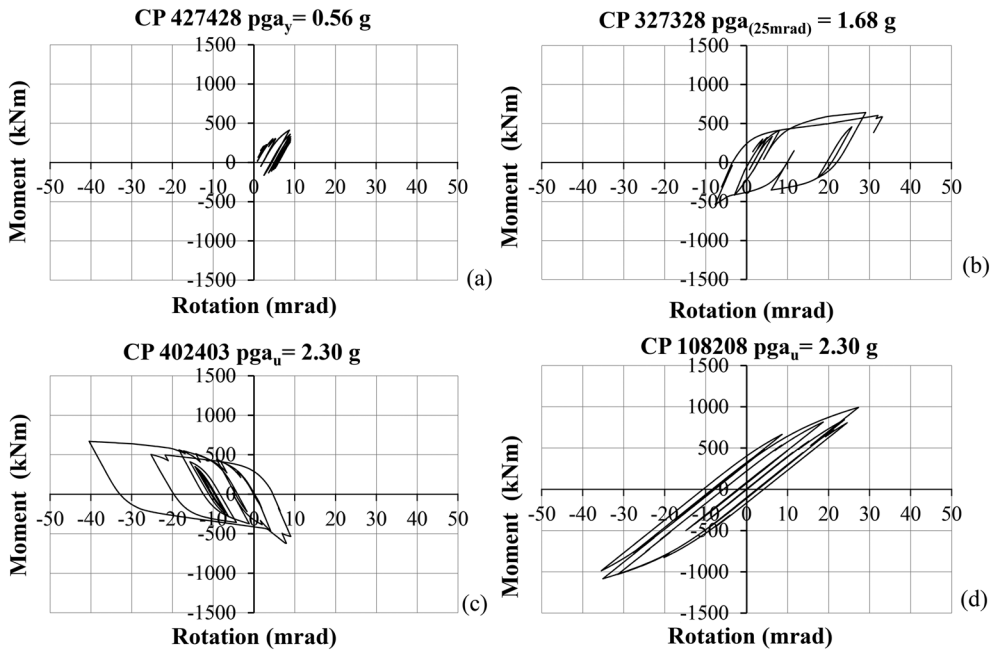


Figure 17. Moment–rotation relationships for MRF-I owing to accelerogram 1 of (a) BTC joint at pga_y , (b) BTC joint at $pga_{(25 \text{ mrad})}$, (c) BTC joint at pga_u and (d) CB at pga_u .

ductility and redundancy—and overstrength values. This finding was also observed in Thermou *et al.* [39] and was mainly caused by code constraints, such as second-order effects and damage limit states for frame structures, that led to overconservative design.

6. CONCLUSIONS

This paper presented the results of an experimental and numerical study that focussed on both the characterisation and modelling of seismic innovative solutions of BTC joints and CB joints made of CFT columns in high-strength steel. Initially and with reference to the experimental performance of BTC joint specimens, one can conclude that the proposed joint typology can achieve plastic rotation values up to 40 mrad; these values are more than adequate for DCM MRFs. Along the same line, CB joint specimens exhibited plastic rotations of about 45 mrad, being so adequate for the aforementioned frames too. In both cases, those maximum rotations were achieved with both strength and stiffness reduction below 20%, in agreement with the requirements of EN1998-1. Then, with regard to columns, non-dissipative members made of high-strength steel represented an economic solution with respect to mild steel owing to their inherent strength that allowed overall cost savings of about 5%. In sum, design formulae included in EN1993-1 and EN1994-1-1 and valid up to steel grades S460 resulted to be suitable for the design of non-dissipative high-strength steel columns analysed in this research work; moreover, plastic global analysis with fully yielded sections was effective for both joints and beams. Finally, the outcomes provided by this paper will allow for the application of the performance-based earthquake technique to 3D reference structures composed by both MRFs and concrete shear walls.

APPENDIX A

A1. Hysteretic models

The hysteretic behaviour for BTC and CB joints was modelled using the Bouc–Wen and the pinching hysteretic model provided by the OpenSees software [34], as shown in Figure A1(a) and (b)

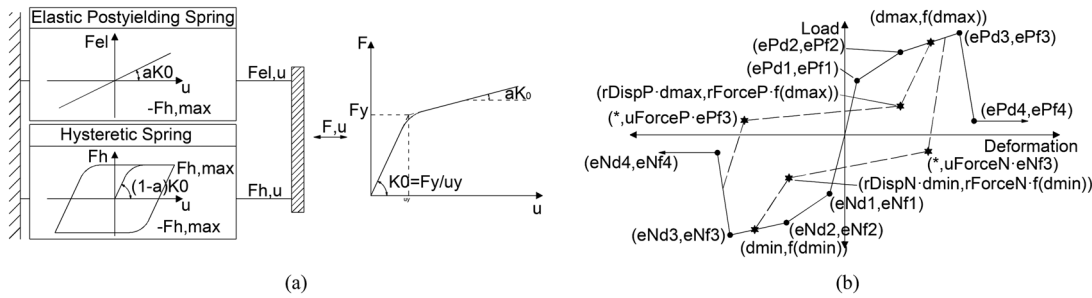


Figure A1. Hysteretic models (a) Bouc-Wen and (b) pinching.

respectively. Both in the simulated BTC joint and in the simulated standard CB joint, the two models were considered to operate in parallel. The Bouc–Wen model provided the main part of actual behaviour, while the pinching model reproduced slip owing to damaged concrete and consequent hardening, additional local stiffness degradation and strength reduction, and the asymmetric behaviour between sagging and hogging moment, as shown in Figure A2. The Bouc–Wen model implemented is an extension of the original model that includes stiffness and strength degradation [40]. The hysteretic model proposed is governed by the following non-linear differential equations:

$$\ddot{m}u + c\dot{u} + [\alpha k u + (1 - \alpha)k z] = -m a \quad (\text{A1})$$

and

$$\dot{z} = \frac{\left[A\dot{u} - v \left(\beta |\dot{u}| |z|^{n-1} z + \gamma \dot{u} |z|^n \right) \right]}{\eta} \quad (\text{A2})$$

where A , β , γ and n are parameters that control the shape of the hysteresis, whilst η and v govern main stiffness and strength degradation phenomena respectively. This model reproduces symmetric cycles and does not take into account pinching effects, as highlighted in Figure A2.

Thus, in order to take into account the amount of slip observed during testing and the asymmetric behaviour of BTC joints owing to the composite steel–concrete section, the pinching model shown in Figure A1(b) was used. Moreover and because of its easier polygonal nature than the smooth Bouc–Wen model, it was also used to take into account both stiffness and strength degradation. Therefore, δA , $\delta \eta$ and δv were assumed to be zero in Equation (A2). In particular, the pinching

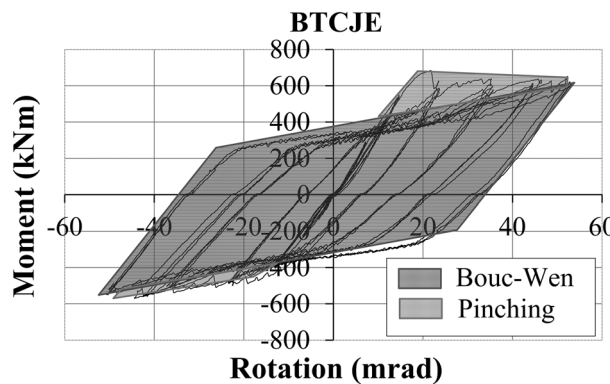


Figure A2. Hysteretic models of BTCJs.

model was governed by means of damage indices δj_i whose general formulation is proposed in Lowes *et al.* [41]:

$$\delta j_i = gj1 \left(\max \left\{ \frac{d_{\max,i}}{def_{\max}}, \frac{d_{\min,i}}{def_{\min}} \right\}^{gj3} \right) + gj2 \left(\frac{\int_{load history} dE_i}{E_{monotonic}} \right)^{gj4} \quad (A3)$$

where $j=k, d$ and f . In particular, the damage models are expressed in terms of damage indices as stiffness degradation δk_i , deformation demand δd_i and strength degradation δf_i , as defined herein:

$$k_i = k_0(1 - \delta k_i) \quad (A4)$$

$$d_{\max,i} = d_{\max,0}(1 - \delta d_i) \quad (A5)$$

$$f_{\max,i} = f_{\max,0}(1 - \delta f_i) \quad (A6)$$

where $gj1, gj2, gj3$ and $gj4$ are degradation model parameters; $E_{monotonic}$ defines the energy required to achieve failure under monotonic loading; k_i is the unloading stiffness at time t_i ; k_0 is the initial unloading stiffness for the case of no damage; def_{\max} and def_{\min} are the positive and negative deformations respectively that define failure; $d_{\max,i}$ and $d_{\min,i}$ are the maximum historic and minimum historic deformation demands; $f_{\max,i}$ is the current envelope maximum strength at time t_i ; and $f_{\max,0}$ is the initial envelope maximum strength for the case of no damage.

The model parameters reported in Tables AI–AVII hereinafter are of two types: (i) dimensionless indices providing the shape of the hysteresis, which is intimately bounded to the joint typologies, and (ii) dimensional indices related to quantitative measures of the cyclic behaviour of the analysed joints. It is clear that a change of the joint size components will correspond to a change in both the linear and the non-linear joint response. However, because the joint typologies involved are the same, once estimated, the elastic properties and plastic moments of new scaled joints, the proposed hysteresis models should be able to reproduce their main cyclic behaviour.

A2. Hysteretic models for BTCJs

Relevant main parameters for BTCJ joints are reported in Tables AI–AIII.

Table AI. Bouc–Wen parameters of BTCJs.

Parameter	Value	Parameter	Value	Parameter	Value
α (-)	0.065	γ (-)	6927	δA (-)	0.00
k_0 (N mm/rad)	0.88E+11	β (-)	6927	δv (-)	0.00
n (-)	1.76	A_0 (-)	1.00	$\delta \eta$ (-)	0.00

Table AII. Pinching parameters of envelope and target points of BTCJs.

Parameter	Value	Parameter	Value	Parameter	Value
$ePf1$ (N mm)	375E+06	$eNf1$ (N mm)	-150E+06	$rDispP$ (-)	0.50
$ePd1$ (rad)	7E-03	$eNd1$ (rad)	15E-03	$rForceP$ (-)	0.25
$ePf2$ (N mm)	333E+06	$eNf2$ (N mm)	-190E+06	$uForceP$ (-)	0.25
$ePd2$ (rad)	12E-03	$eNd2$ (rad)	-20E-03	$rDispN$ (-)	0.50
$ePf3$ (N mm)	295E+06	$eNf3$ (N mm)	-180E+06	$rForceN$ (-)	0.25
$ePd3$ (rad)	32E-03	$eNd3$ (rad)	-30E-03	$uForceN$ (-)	0.25
$ePf4$ (N mm)	180E+06	$eNf4$ (N mm)	-130E+06		
$ePd4$ (rad)	42E-03	$eNd4$ (rad)	-40E-03		

Table AII. Pinching parameters of damage index of a BTCJs.

Parameter	Value	Parameter	Value	Parameter	Value
$gK1$ (-)	0.25	$gD1$ (-)	0.50	$gF1$ (-)	0.70
$gK2$ (-)	0.35	$gD2$ (-)	0.50	$gF2$ (-)	0.00
$gK3$ (-)	0.40	$gD3$ (-)	2.00	$gF3$ (-)	0.60
$gK4$ (-)	0.20	$gD4$ (-)	2.00	$gF4$ (-)	0.70
gKL (-)	0.50	gDL (-)	0.50	gFL (-)	0.90

A3. Hysteretic models for CBJSEs

Relevant main parameters for CBJSE joints are reported in Tables AIV–AVI.

Table AIV. Bouc–Wen parameters of CBJSEs.

Parameter	Value	Parameter	Value	Parameter	Value
α (-)	0.05	γ (-)	117 065.5	δA (-)	0.00
k_0 (N mm/rad)	1.6E+11	β (-)	117 065.5	δv (-)	0.00
n (-)	2.00	A_0 (-)	1.00	$\delta \eta$ (-)	0.00

Table AV. Pinching parameters of envelope and target point CBJSEs.

Parameter	Value	Parameter	Value	Parameter	Value
$ePf1$ (N mm)	400E+06	$eNf1$ (Nmm)	-400E+06	$rDispP$ (-)	0.45
$ePd1$ (rad)	3E-03	$eNd1$ (rad)	-3E-03	$rForceP$ (-)	0.30
$ePf2$ (N mm)	850E+06	$eNf2$ (N mm)	-850E+06	$uForceP$ (-)	-0.375
$ePd2$ (rad)	10E-03	$eNd2$ (rad)	-9E-03	$rDispN$ (-)	0.4531
$ePf3$ (N mm)	900E+06	$eNf3$ (N mm)	-900E+06	$rForceN$ (-)	0.30
$ePd3$ (rad)	50E-03	$eNd3$ (rad)	-50E-03	$uForceN$ (-)	-0.3929
$ePf4$ (Nmm)	500E+06	$eNf4$ (Nmm)	-400E+06		
$ePd4$ (rad)	80E-03	$eNd4$ (rad)	-80E-03		

Table AVI. Pinching parameters of damage index of the CBJSEs.

Parameter	Value	Parameter	Value	Parameter	Value
$gK1$ (-)	0.25	$gD1$ (-)	0.80	$gF1$ (-)	1.00
$gK2$ (-)	1.00	$gD2$ (-)	0.80	$gF2$ (-)	1.00
$gK3$ (-)	1.00	$gD3$ (-)	0.80	$gF3$ (-)	1.00
$gK4$ (-)	1.00	$gD4$ (-)	0.80	$gF4$ (-)	1.00
gKL (-)	0.80	gDL (-)	1.00	gFL (-)	0.25

A4. Hysteretic models for CBJINs

Relevant main parameters for CBJIN joints are reported in Table AVII. In this particular case, the pinching model of Figure A1(b) was not employed because slip effects associated with end columns embedded in the foundation were negligible.

Table AVII. Bouc–Wen parameters of CBJINs.

Parameter	Value	Parameter	Value	Parameter	Value
α (-)	0.28739	γ (-)	97514.2	δA (-)	0.00
k_0 (N mm/rad)	0.40E+11	β (-)	97514.2	δv (-)	0.00
n (-)	3.30	A_0 (-)	1.00	$\delta \eta$ (-)	0.00

ACKNOWLEDGEMENTS

This work was carried out with a financial grant from the RFCS of the European Community, within the ATTEL project ‘Performance-Based Approaches for High Strength Steel Tubular Columns and Connections under Earthquake and Fire Loadings’, Grant No RFSR-CT-2008-00037. The financial support of the Province of Trento through the Call 3—post-doc 2009 (outgoing)—FIRAS project “Performance-based analysis of fire and seismic resistance of steel-concrete composite structures” is also gratefully acknowledged.

REFERENCES

1. EN1993-1-12. *Eurocode 3 - Design of Steel Structures - Part 1-12: Additional Rules for the Extension of EN 1993 up to Steel Grades S 700*. CEN: Bruxelles, 2007.
2. Hoang VL, Demonceau JF, Ly DPL, Rossi B. Field of application of high strength steel circular tubes for steel and composite columns from an economic point of view. *Journal of Constructional Steel Research* 2011; **67**:1001–1021.
3. Moze P, Beg D. High strength steel tension splices with one or two bolts. *Journal of Constructional Steel Research* 2010; **66**:1000–1010.
4. Puthli R, Fleischer O. Investigations on bolted connections for high strength steel members. *Journal of Constructional Steel Research* 2001; **57**:313–326.
5. Jiao H, Zhao X-L. Imperfection, residual stress and yield slenderness limit of very high strength (VHS) circular steel tubes. *Journal of Constructional Steel Research* 2003; **59**:233–249.
6. Tondini N, Hoang VL, Demonceau J-F, Franssen J-M. Experimental and numerical investigation of high-strength steel circular columns subjected to fire. *Journal of Constructional Steel Research* 2013; **80**:57–81.
7. Mursi M, Uy B. Strength of slender concrete filled high strength steel box columns. *Journal of Constructional Steel Research* 2004; **60**:1825–1848.
8. Uy B. Strength of short concrete filled high strength steel box columns. *Journal of Constructional Steel Research* 2001; **57**:113–134.
9. Silva AT, Rebelo C, Silva LS, Serra M, Lima LRO, D’Aniello M, Landolfo R. Seismic performance of high-strength steel moment-resisting frames. Proceedings of Behaviour of Steel Structures in Seismic Areas: STESSA 2012, 2012, Santiago, Chile, January 9 – 11.
10. Wang W, Chen Y, Li W, Leon RT. Bidirectional seismic performance of steel beam to circular tubular column connections with outer diaphragm. *Earthquake Engineering & Structural Dynamics* 2011; **40**:1063–1081. DOI: 10.1002/eqe.1070.
11. Jaspart J-P, Demonceau J-F, Bursi OS et al. Performance-based approaches for high strength tubular columns and connections under earthquake and fire loadings. Final Report, ATTEL Project, Contr. No: RFSR-CT-2008-00037, Research Fund for Coal and Steel, 2011.
12. Tagawa H, MacRae G, Lowes L. Probabilistic evaluation of seismic performance of 3-story 3D one- and two-way steel moment-frame structures. *Earthquake Engineering & Structural Dynamics* 2008; **37**:681–696. DOI: 10.1002/eqe.778.
13. SEOAC Vision 2000 Committee. *Performance-Based Seismic Engineering*. Structural Engineering Association of California: Sacramento, California, 1995.
14. Foley CM, Pezeshk S, Alimoradi A. Probabilistic performance-based optimal design of steel moment-resisting frames. I: formulation. *Journal of Structural Engineering* 2007; **133**(6):757–766.
15. Alimoradi A, Pezeshk S, Foley CM. Probabilistic performance-based optimal design of steel moment-resisting frames. II: applications. *Journal of Structural Engineering* 2007; **133**(6):767–776.
16. Cornell CA, Jalayer F, Hamburger RO, Foutch DA. Probabilistic basis for 2000 SAC Federal Emergency Management Agency steel moment frame guidelines. *Journal of Structural Engineering* 2002; **128**(4):526–533.
17. Lee T-H, Mosalam KM. Probabilistic seismic evaluation of reinforced concrete structural components and systems. Pacific Earthquake Engineering Research Center, PEER, Report n. 2006/04.
18. Hidalgo PA, Jordan RM, Martinez MP. An analytical model to predict the inelastic seismic behavior of shear-wall, reinforced concrete structures. *Engineering Structures* 2002; **24**:85–98.
19. Jalali A, Dashti F. Nonlinear behavior of reinforced concrete shear walls using macroscopic and microscopic models. *Engineering Structures* 2010; **32**:2959–2968.
20. Kazaz I, Gülkán P, Yakut A. Performance limits for structural walls: an analytical perspective. *Engineering Structures* 2012; **43**:105–119.
21. Rutenberg A, Nsieri E. The seismic shear demand in ductile cantilever wall systems and the EC8 provisions. *Bulletin of Earthquake Engineering* 2006; **4**:1–21. DOI: 10.1007/s10518-005-5407-9.
22. Pucinotti R, Bursi OS, Franssen J-M, Lennon T. Seismic-induced fire resistance of composite welded beam-to-column joints with concrete filled tubes. *Fire Safety Journal* 46 2011; **6**(2011):335–347.
23. EN1998-1. *Eurocode 8: Design of Structures for Earthquake Resistance - Part 1: General Rules, Seismic Actions and Rules for Buildings*. CEN: Bruxelles, 2004.
24. Johansson B, Collin P. *Eurocode for High Strength Steel and Application in Construction*. Lulea, University of technology: Sweden, 2006.
25. Alosta YM, Schneider SP. Analytical behavior of connections to concrete-filled steel tubes. *Journal of Constructional Steel Research* 1996; **40**(2):95–127.
26. Pucinotti R, Bursi OS, Demonceau J-F. Post-earthquake fire and seismic performance of welded steel-concrete composite beam-to-column joints. *Journal of Constructional Steel Research* 2011; **67**(9):1358–1375.

27. EN1993-1-8. *Eurocode 3 – Design of Steel Structures – Part 1-8: Design of Joint*. EN 1993-1-8; CEN: Bruxelles, 2007.
28. EN1992-1-1. *Eurocode 2 - Design of Concrete Structures - Part 1-1: General Rules and Rules for Buildings*. EN 1992-1-1; CEN: Bruxelles, 2005.
29. Hibbit Karlsson and Sorensen. ABAQUS user's manuals. 1080 Main Street, Pawtucket, R.I. 02860 2000.
30. EN ISO 6892-1. *Metallic Materials - Tensile Testing - Part 1: Method of Test at Ambient Temperature* CEN: Bruxelles, 2009.
31. EN10025-2. *Hot Rolled Products of Structural Steels - Part 2: Technical Delivery Conditions for Non-alloy Structural Steels*. CEN: Bruxelles, 2004.
32. ECCS. *Recommended Testing Procedure for Assessing the Behaviour of Structural Steel Elements Under Cyclic Loads*. ECCS Publication n° 45; ECCS: Bruxelles, 1986.
33. SAC. Protocol for fabrication, inspection, testing, and documentation of beam-column connection tests and other experimental specimens. Report n. SAC /BD-97/02, 1997.
34. Mazzoni S, McKenna F, Scott MH, Fenves GL. *OpenSees Command Language Manual*. Pacific Earthquake Engineering Research Center: University of California, Berkeley, 2007.
35. Sozonov P, Pucinotti R, Tondini N, Bursi OS, Zanon G. Probabilistic seismic analysis of a three-dimensional steel-concrete composite structure. Proceedings of the Twelfth International Conference on Computational Structures Technology, Naples, 2-5 September, 2014.
36. EN1994-1-1. *Eurocode 4: Design of Composite Steel and Concrete Structures - Part 1-1: General Rules for Buildings*, CEN: Bruxelles, 2005.
37. FEMA-356. *Prestandard and Commentary for the Seismic Rehabilitation of Buildings*. FEMA: Washington, USA, 2000.
38. Bursi OS, Zandonini R, Salvatore W, Caramelli S, Haller M. Seismic behavior of a 3D full-scale steel-concrete composite moment resisting frame structure. *Proceedings of Fifth International Conference on Composite Construction in Steel and Concrete* 2006; 641–652.
39. Thermou GE, Elhashai AS, Plumier A, Doneux C. Seismic design and performance of composite frames. *Journal of Constructional Steel Research* 2004; **60**:31–57.
40. Baber TT, Wen YK. Post-earthquake random vibrations of hysteretic degrading systems. *Journal of Engineering Mechanics* 1981; **107**(EM6):1069–1089.
41. Lowes LN, Mitra N, Altoontash A. A beam-column joint model for simulating the earthquake response of reinforced concrete frames, Pacific Earthquake Engineering Research Center, PEER. Report n. 2003/10.
42. Vamvatsikos D, Cornell CA. Incremental dynamic analysis. *Earthquake Engineering & Structural Dynamics* 2002; **31**:491–514. DOI: 10.1002/eqe.141.